

Origin of enhanced charge density wave in the kagome superconductor $\text{CsV}_{3-x}\text{Mo}_x\text{Sb}_5$

Jiangpeng Song^{1,2}, Tao Han², Zekun Zhou², Qingge Mu², Xingyuan Hou², Zongyuan Zhang², Yubing Tu², and Lei Shan^{2,3,*}

¹*School of Materials Science and Engineering, Anhui University, Hefei 230601, China*

²*Information Materials and Intelligent Sensing Laboratory of Anhui Province, Institutes of Physical Science and Information Technology, Anhui University, Hefei 230601, China*

³*Key Laboratory of Structure and Functional Regulation of Hybrid Materials of Ministry of Education, Anhui University, Hefei 230601, China*



(Received 19 June 2024; accepted 9 August 2024; published 22 August 2024)

The topological kagome superconductor CsV_3Sb_5 exhibits rich quantum phenomenology of correlated electronic phases including unconventional charge order and superconductivity. Understanding how the singularities inherent to the kagome lattice are linked to the observed many-body phases is a topic of great interest. Here, by using Shubnikov–de Haas oscillation measurements, we report the detailed evolution of electronic band structures in $\text{CsV}_{3-x}\text{Mo}_x\text{Sb}_5$ single crystals, where Mo substitution causes a suppression of superconductivity and an enhanced charge density wave. The obvious decrease of oscillation frequency (F_β) corresponding to the nontrivial band from 72 to 59 T and smaller cyclotron effective mass ($\sim 0.069m_e$) reveal that the van Hove singularities from the vanadium orbitals near M are abnormally lifted and promote the nesting condition for the charge density wave. Meanwhile, the electric conduction changes from a hole-dominated multiband feature to a single electron band feature and the anomalous Hall effect becomes stronger. In conjunction with the simple schematics of band structures, the promoted Fermi-surface nesting is dominant in the unusual enhanced charge density wave, offering insight to comprehend the delicate interaction between the intertwined orders in this kagome system.

DOI: [10.1103/PhysRevB.110.054518](https://doi.org/10.1103/PhysRevB.110.054518)

I. INTRODUCTION

Kagome compounds have attracted enormous interest as they offer a fertile ground to investigate exotic quantum phenomena, such as charge density wave (CDW), superconductivity, van Hove singularity (VHS), nontrivial topological bands, and geometrically frustrated magnetism [1–3]. The flat bands and VHSs naturally promote the strong electronic correlations in the band structure of a kagome lattice [4]. When the flat band is located at E_F , ferromagnetism and the fraction quantum Hall effect could appear in these kagome metals [5]. In correlated systems, Coulomb interactions between electrons at the VHS would exceed their kinetic energy and drive multiple instabilities [6,7]. However, materials with the VHSs near E_F are rare. Recently, vanadium-based kagome superconductors AV_3Sb_5 ($A = \text{K/Rb/Cs}$) are found and show numerous exotic physical properties, such as superconductivity ($T_c \sim 0.9\text{--}2.7$ K), CDW order ($T_{\text{CDW}} \sim 78\text{--}103$ K), and anomalous Hall effect with the absence of local moments or magnetic correlations, etc. [8–13].

CsV_3Sb_5 , the first member of AV_3Sb_5 compounds, exhibits the highest superconducting transition temperature and multiple electronic instabilities compared with other members [8]. Under pressure and chemical doping with the Nb, Ta, Ti, and Sn elements, the CDW order is suppressed while the superconductivity is enhanced or exhibits a double-dome behavior, suggesting that the CDW instability seemingly

competes with superconductivity [14–18]. Meanwhile, the recent theoretical predictions explain that the charge order at T_{CDW} can be understood as arising from the Fermi-surface nesting at the VHSs in CsV_3Sb_5 [19]. In spite of extensive progress in both theories and experiments for CsV_3Sb_5 [14,20–22], the physical mechanisms, for example, the competition between superconductivity and different charge orders, the origin of the unusual superconducting phase diagram with a double-dome character and the role of each VHS in these competing orders remain elusive. In contrast with the other doped cases of CsV_3Sb_5 , the Mo-doped case is extraordinary, in that the T_{CDW} is increased while the superconductivity is suppressed [23–25]. It is important to identify the origin of enhanced CDW in Mo-doped CsV_3Sb_5 . The detection of quantum oscillations by Mo doping through tuning the chemical pressure or carrier concentrations in a crystal is an effective method to probe the detailed Fermi-surface evolution [26], which can provide valuable insights into the interplay between the CDW order and superconductivity.

In this work, we present the detailed evolution of electronic band structures by probing the Shubnikov–de Haas (SdH) oscillations using high-quality single crystals of $\text{CsV}_{3-x}\text{Mo}_x\text{Sb}_5$ ($0 \leq x \leq 0.10$). With the increase of Mo content, the CDW order is enhanced and the superconductivity is suppressed. The analysis of SdH oscillations reveals the obvious shrinkage of the Fermi surface corresponding to F_β and a subtle change of the Fermi surface corresponding to F_α . The Hall measurements show the change of the electrical transport process and the anomalous Hall effect. More introduced

*Contact author: lshan@ahu.edu.cn

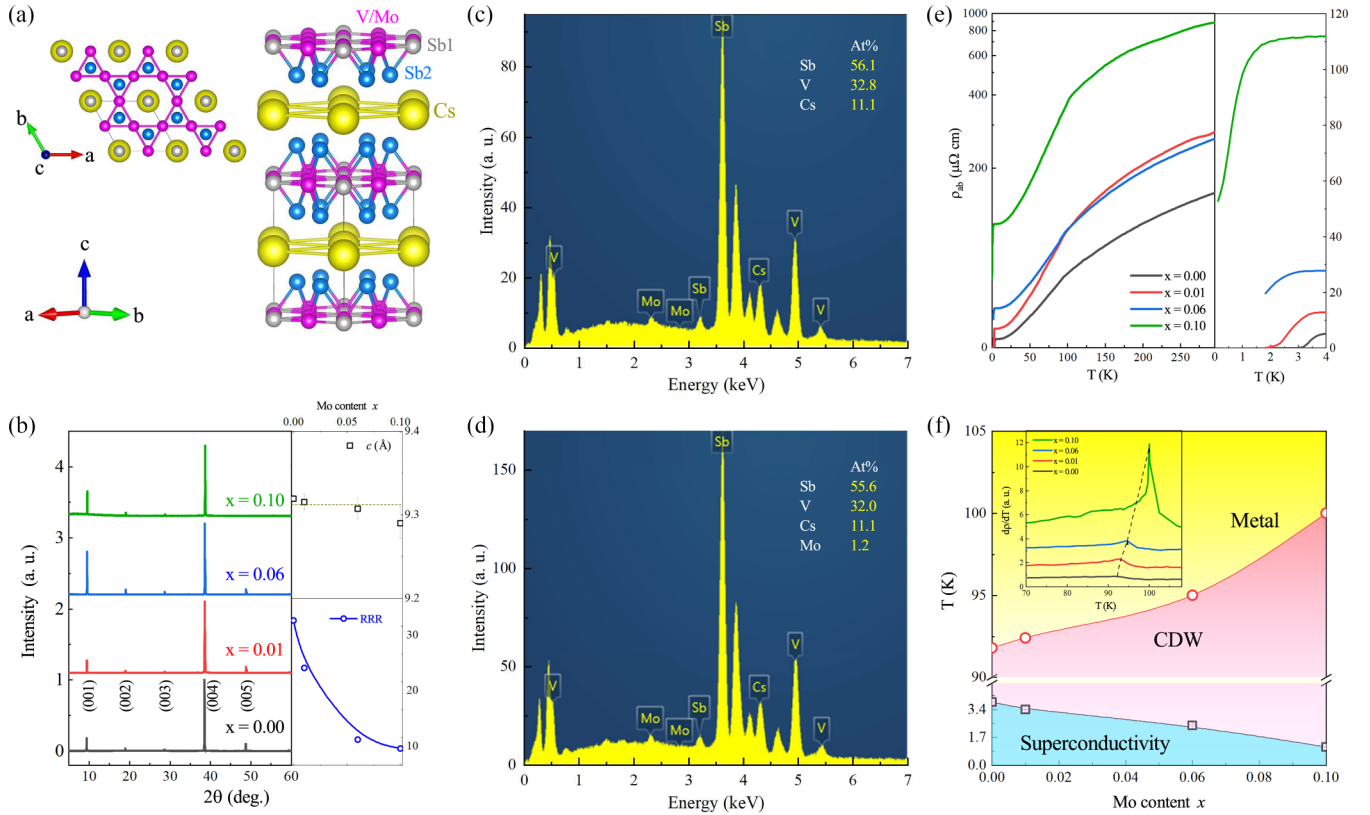


FIG. 1. (a) Crystal structures of $\text{CsV}_{3-x}\text{Mo}_x\text{Sb}_5$. (b) Single-crystal x-ray diffraction pattern, the lattice parameter c , and the residual resistivity ratio for $\text{CsV}_{3-x}\text{Mo}_x\text{Sb}_5$. (c) EDS of CsV_3Sb_5 single crystal. (d) EDS of $x = 0.10$ single crystal. (e) Temperature-dependent in-plane resistivity of $\text{CsV}_{3-x}\text{Mo}_x\text{Sb}_5$ single crystals. (f) Phase diagram of $\text{CsV}_{3-x}\text{Mo}_x\text{Sb}_5$, which illustrates the evolution of CDW and superconductivity. Inset: Temperature dependence of $d\rho/dT$ curves.

electrons and modifications to the band structure will enlarge the Fermi surface centered around Γ . As such, compared with the other cases of substituted CsV_3Sb_5 , our results reveal that Mo substitution causes the antiphase shift of the Sb-derived electron band near Γ and the V-derived band forming the VHSs near M , unveiling that VHS from d_{xz}/d_{yz} vanadium orbitals plays an important role in the Fermi-surface nesting, which is dominant in the electronic instabilities of $\text{CsV}_{3-x}\text{Mo}_x\text{Sb}_5$.

II. EXPERIMENTAL METHODS

Single crystals of $\text{CsV}_{3-x}\text{Mo}_x\text{Sb}_5$ were grown by the self-flux method as referred from Ref. [8]. The x-ray diffraction (XRD) with $\text{Cu } K\alpha$ radiation was used to characterize the crystal structure. Energy dispersive x-ray spectroscopy (EDS) and inductively coupled plasma atomic emission spectroscopy (ICP-AES) were used to characterize the chemical composition of single crystals. The measurements of electrical transport were performed by using the four-probe dc technique in the ab plane on a Quantum Design physical property measurement system (PPMS-DynaCool) (0–14 T). In order to avoid the effect caused by electrode asymmetry, the transport data were measured under both positive and negative magnetic fields.

III. RESULTS AND DISCUSSIONS

The side and top views of the layered crystal structure for $\text{CsV}_{3-x}\text{Mo}_x\text{Sb}_5$ are displayed in Fig. 1(a). The V/Mo sublattice forms a two-dimensional kagome lattice and the V_3Sb_5 slabs are intercalated by alkali metal cations. We first characterize the crystal structure by XRD measurements. Figure 1(b) shows the single-crystal XRD patterns of $\text{CsV}_{3-x}\text{Mo}_x\text{Sb}_5$ samples with x from 0 to 0.10. The actual elemental compositions of all our samples are determined by EDS and ICP-AES measurements. EDS data of pristine CsV_3Sb_5 and $x = 0.10$ samples are shown in Figs. 1(c) and 1(d). The accurate doping contents of $x = 0.01$ and $x = 0.06$ samples are determined from the ICP-AES. The observable (00 l) diffraction peaks indicate that the c axis is perpendicular to the cleaved planes of single crystals. In previous reports of other doped systems, the lattice parameter c remains almost the same for the cases of Nb-, Ta-, and Cr-doped CsV_3Sb_5 , where these doped systems mainly affect the lattice parameters in the ab plane [17,18,27]. As shown in the upper right part of Fig. 1(b), the lattice parameter c changes a little when errors are considered, and is slightly reduced from 9.31(9) to 9.29(0) Å with increasing Mo content. Even though the radius of Mo is larger than the radius of V, the c presents a decreasing trend. Further experiments are required to confirm and clarify this result.

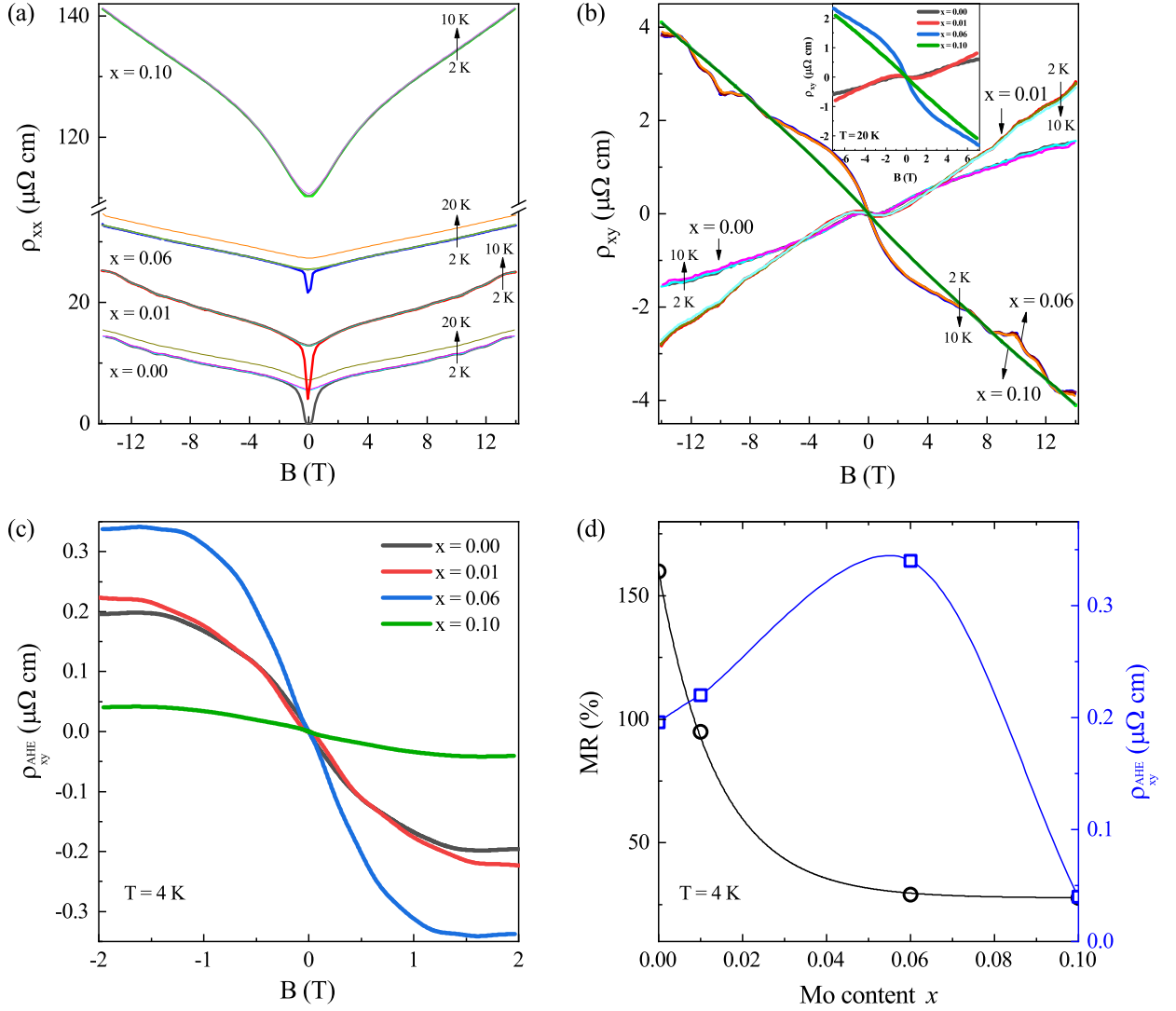


FIG. 2. (a) Field dependence of in-plane resistivity for $\text{CsV}_{3-x}\text{Mo}_x\text{Sb}_5$ up to 14 T at various temperatures. (b) Field dependence of Hall resistivity for $\text{CsV}_{3-x}\text{Mo}_x\text{Sb}_5$ up to 14 T from 2 to 10 K. Inset: Field dependence of Hall resistivity up to 7 T at 20 K. (c) The extracted anomalous Hall resistivity (ρ_{xy}^{AHE}) by subtracting the local linear ordinary Hall background at 4 K for $\text{CsV}_{3-x}\text{Mo}_x\text{Sb}_5$. (d) Magnetoresistance and the saturated ρ_{xy}^{AHE} as a function of Mo content x .

Temperature dependence of the in-plane resistivity ρ_{ab} for $\text{CsV}_{3-x}\text{Mo}_x\text{Sb}_5$ is shown in Fig. 1(e). The resistivity of pristine CsV_3Sb_5 exhibits a clear shoulder near 92.0 K due to the formation of a CDW order in the kagome plane and zero resistivity below the temperature ~ 2.72 K. With increasing x , the residual resistivity ratio (RRR) of $\text{CsV}_{3-x}\text{Mo}_x\text{Sb}_5$ is systematically reduced in the lower right part of Fig. 1(b), implying a stronger scattering effect in the crystal structure after doping. Figure 1(f) summarizes the phase diagram about superconductivity and CDW at different Mo doping levels. It is obvious that the CDW transition temperature increases from 92 K for the pristine CsV_3Sb_5 sample to 100 K for the $x = 0.10$ sample. As the enhanced T_{CDW} , we now turn to the evolution of superconductivity to understand the interplay with the CDW order. Here, we define T_c from the resistivity data by the criterion of $90\% \rho_N$ (ρ_N represents the normal-state resistivity). One can see that T_c exhibits monotonic suppressed

behavior with increasing x and reaches a minimum value of about 1.1 K for the $x = 0.10$ sample. This competition picture between superconductivity and CDW order is analogous to the pressurized and chemical doped experiments [14–18].

The magnetoresistivity and Hall measurements under external magnetic field in the ab -plane of $\text{CsV}_{3-x}\text{Mo}_x\text{Sb}_5$ are shown in Figs. 2(a) and 2(b). The Hall signal exhibits an antisymmetric S shape at the low-field region (0–2 T) for pristine CsV_3Sb_5 and doped samples, which is attributed to an anomalous Hall effect (AHE) according to previous reports [11]. For $x = 0.06$ and $x = 0.10$ samples, the Hall signals become negative through the whole field range, indicating that the conduction changes from the hole-dominated multi-band feature of pristine CsV_3Sb_5 to the single electron band feature in this electron-doped case. The overall evolution of the Hall signal is consistent with the recently reported data in Mo-doped CsV_3Sb_5 [25]. As shown in Fig. 2(c),

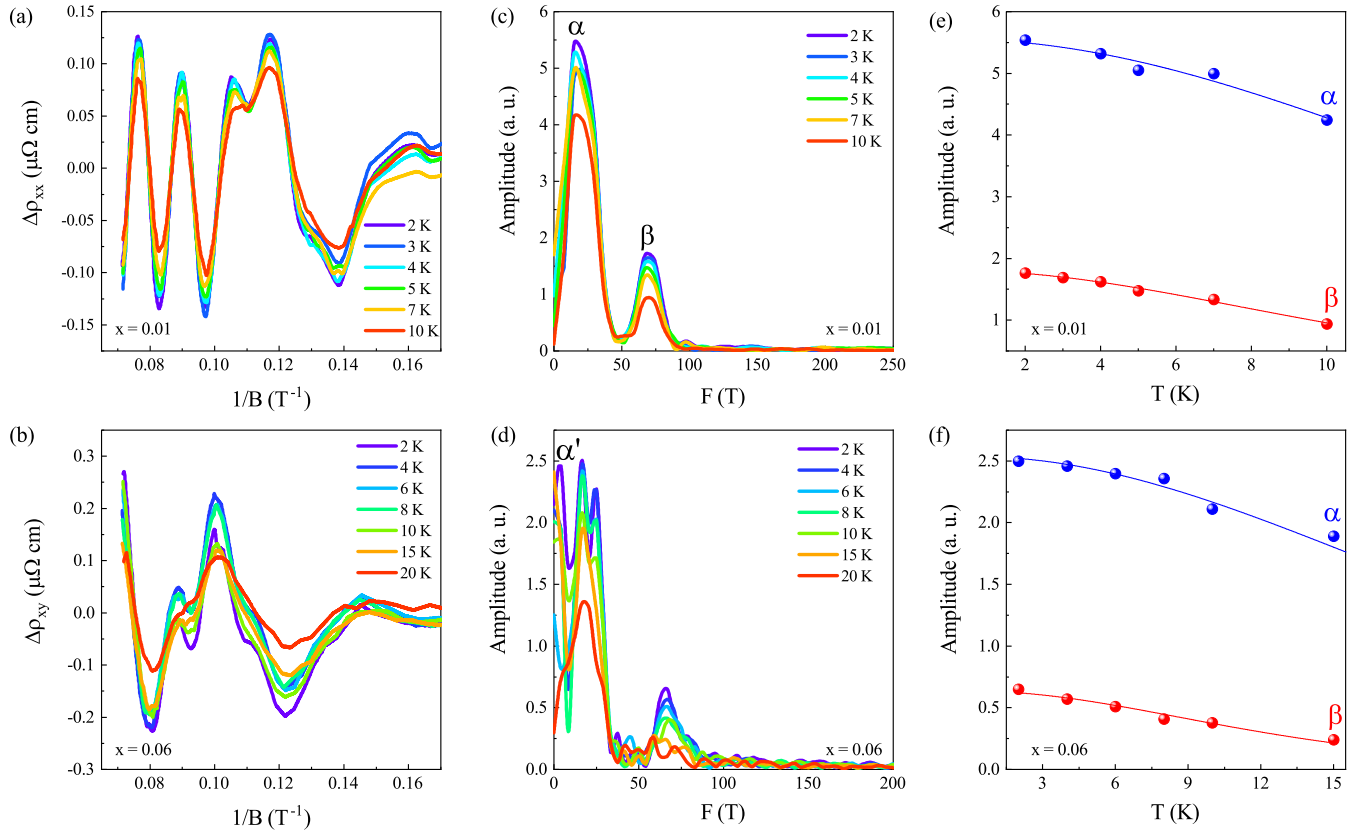


FIG. 3. (a) and (b) The oscillatory parts after subtracting a background as a function of $1/B$ at various temperatures for $x = 0.01$ and $x = 0.06$ samples, respectively. (c) and (d) The fast Fourier transform spectra from (a) and (b) at different temperatures, which show that Fourier transform amplitude decreases at high temperatures. (e) and (f) The Fourier transform amplitude as a function of temperature for F_α and F_β . The solid lines are the fitting curves by the LK formula.

the AHE signals (ρ_{xy}^{AHE}) at 4 K are extracted by subtracting the local linear Hall background. We summarize the changes of magnetoresistance ($\text{MR} = [\rho(H) - \rho(0)]/\rho(0)$) and ρ_{xy}^{AHE} in Fig. 2(d). The values of MR and RRR [as seen in Fig. 1(b)] monotonically decrease with the Mo doping due to the disorder scattering in crystal structures. It is shown that the enhanced ρ_{xy}^{AHE} for $x = 0.01$ and $x = 0.06$ samples are consistent with the increase of CDW transition temperature. However, ρ_{xy}^{AHE} abruptly drops at $x = 0.10$, which could be attributed to the change of the dominant carrier type or detailed changes of electronic band structure by Mo doping. According to the previous reports, such as Nb- and Cr-doped systems, the AHE signal accompanying the CDW order in CsV_3Sb_5 is explained that the possible existence of a chiral flux phase breaks time-reversal symmetry [17,27]. Although the origin of AHE is still under debate, $\text{CsV}_{3-x}\text{Mo}_x\text{Sb}_5$ provides a further platform for understanding the expected chiral CDW scenario.

A detailed evolution of the electronic band structure is important for understanding the interplay between different charge orders in the CsV_3Sb_5 family. Quantum oscillation is a powerful tool to probe the actual Fermi surface reflecting the information of the Fermi-surface evolution and their quasiparticle effective masses. In Figs. 2(a) and 2(b), clear Shubnikov–de Haas (SdH) oscillations can be observed at 2 K under an external magnetic field and become weaker with an

increase of Mo content. The quantum oscillation analysis of the pristine CsV_3Sb_5 has been widely reported [28–32], so we focus here on the experimental results after Mo doping. By subtracting the background, the oscillatory parts of magnetoresistivity for $x = 0.01$ and Hall resistivity for $x = 0.06$ as a function of inverse field ($1/B$) at several representative temperatures are plotted in Figs. 3(a) and 3(b), respectively. In principle, the fast Fourier transform (FFT) of quantum oscillations can directly provide information about the Fermi surfaces. The Fourier transform spectra reveal two distinct frequencies at ~ 17 T (F_α) and ~ 72 T (F_β) in Fig. 3(c). Another lowest oscillatory frequency α' (~ 2.15 T) of the $x = 0.06$ sample is observed in Fig. 3(d), which could originate from the reconstructed small Fermi pockets below T_{CDW} after Mo doping. Although four dominant frequencies are observed in the $x = 0.06$ sample, only two broad peaks of frequencies are distinguished in pristine CsV_3Sb_5 , $x = 0.01$ and $x = 0.10$ samples [as seen in Figs. 4(b) and 4(c)], due to the mixed effect of two close frequencies. The splitting of the peak in the $x = 0.06$ sample could be attributed to a slight warping of the Fermi surface along the c axis, which results in two extremal Fermi-surface areas and therefore two close frequencies [29]. Our results are well consistent with previous SdH experiments and calculations based on a $2 \times 2 \times 2$ CDW [28,29,33].

The cyclotron effective mass m^* can be obtained from the temperature dependence of the Fourier transform amplitude

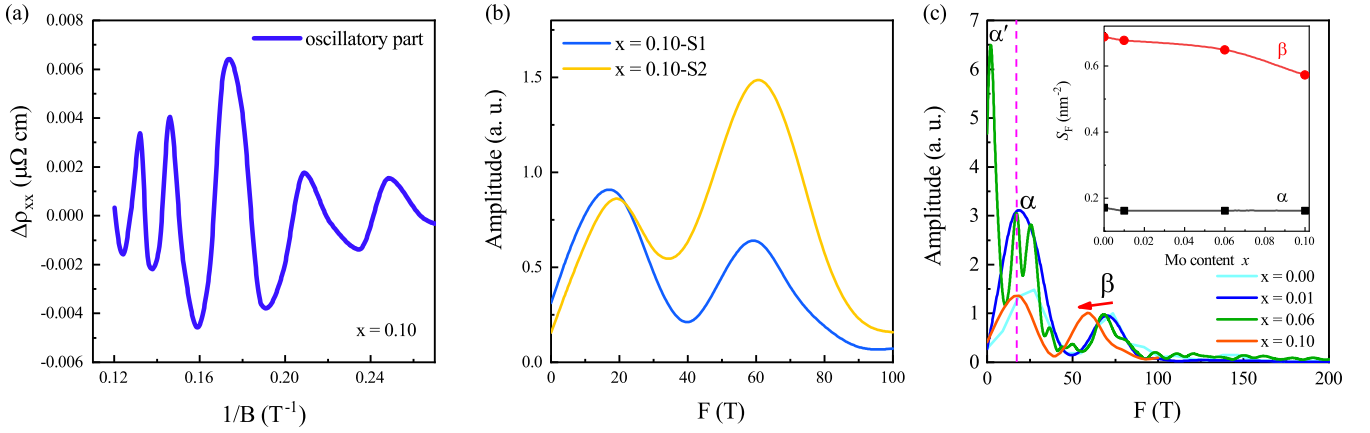


FIG. 4. (a) The oscillatory part after subtracting a background is plotted as a function of $1/B$ for the $x = 0.10$ sample. (b) The Fourier transform spectra for two $x = 0.10$ samples. (c) Doping evolution of the Fourier transform spectra for $\text{CsV}_{3-x}\text{Mo}_x\text{Sb}_5$ ($0 \leq x \leq 0.10$). Inset: The extremal cross sections of Fermi surfaces vs Mo content x for F_α and F_β , respectively.

using the thermal damping term of the Lifshitz-Kosevich (LK) formalism [34], $R_T = X/\sinh X$ with $X = 14.693m^*T/B$ (B is the average value of the magnetic field window). For pristine CsV_3Sb_5 , the effective masses are $0.066m_e$ (m_e is the mass of the free electron) for the α band and $0.10m_e$ for the β band, respectively. As analyzed in Fig. 3(e), the values of m_α^* and m_β^* are $0.063m_e$ and $0.10m_e$ for the $x = 0.01$ sample, which are very close to that of the pristine CsV_3Sb_5 . For the $x = 0.06$ sample, the estimated values of m_α^* and m_β^* are $0.036m_e$ and $0.069m_e$. All these values of m^* are less than $0.10m_e$, reflecting the existence of Dirac bands below T_{CDW} . The effective mass of the $x = 0.10$ sample cannot be obtained because the oscillation signals are very weak. In recent experimental results of topological properties for CsV_3Sb_5 , the Fermi surface corresponding to F_β is demonstrated as a nontrivial band with the Dirac-like crossing [28]. Here, the cyclotron effective mass of the topological β band becomes smaller with the increase of Mo content, revealing that Mo doping pushes the Dirac node close to the Fermi level.

In order to identify the role of VHSs and their interplay with the CDW order and superconductivity, we summarize the change of Fourier transform spectra in $\text{CsV}_{3-x}\text{Mo}_x\text{Sb}_5$, as shown in Fig. 4(c). According to the Onsager relation [34], $F = S_F \hbar / 2\pi e$ (S_F is the extremal cross section of the Fermi surface), the frequencies of quantum oscillations are proportional to the areas of the extremal orbits. In the inset of Fig. 4(c), the obtained values of S_F exhibit a little change for the low-frequency with α band and a distinct decrease for the high-frequency with β band. To understand the results of SdH oscillations, the schematic of change in band structures is shown in Fig. 5. In combination with the previous angle-resolved photoemission spectra (ARPES) reports and theoretical analysis of CsV_3Sb_5 [28,33,35,36], the tiny Fermi surface (F_α) is located in the direction of Γ - K line and the small topological Fermi surface (F_β) is located around the L point.

It has been suggested that the VHSs at the M point near the Fermi level play crucial roles in the formation of the unconventional CDW order and are considered as a driving source for superconductivity in pristine CsV_3Sb_5 [37–39]. Experimentally, hole doping would push the VHSs at the M point above the Fermi level and suppress the CDW order,

such as the Ti-doped case [40]. The VHS at the M point is pushed close to and above the Fermi level in Ta-doped and Nb-doped systems [17,18,36], respectively. Intriguingly, for both $\text{CsV}_{3-x}\text{Ta}_x\text{Sb}_5$ and $\text{CsV}_{3-x}\text{Nb}_x\text{Sb}_5$, the CDW transition temperature is decreased and T_c is increased. When the CDW order is suppressed, the T_c is related to the position of VHSs near the Fermi level in $\text{CsV}_{3-x}\text{Ta}_x\text{Sb}_5$ or the competing incommensurate, quasi-one-dimensional (1D) charge correlations in $\text{CsV}_3\text{Sb}_{5-x}\text{Sn}_x$ [18,41]. As shown in Fig. 5(a), the overall band structure of CsV_3Sb_5 shows a clear modification after Ta doping. Compared with the Ta-doped and Nb-doped systems, Mo doping acts as an electron donor, and its VHSs at the M point are expected to move away from the Fermi level. A simple schematic of the detailed changes in the band structures from CsV_3Sb_5 to Mo-doped samples is plotted in Fig. 5(b). From our SdH experiments, the Fermi surface at the L point becomes smaller and its associated VHS₂ from the d_{xz}/d_{yz} vanadium orbitals at the M point is close to the Fermi level under Mo doping. Meanwhile, the Fermi surface at the Γ - K direction exhibits little change upon Mo substitution.

In the latest strain tuned report, the obvious CDW response to lattice perturbations with the coexistence of a star-of-David pattern and an inverse star-of-David pattern suggests that the high-order VHS₁ from the $d_{xy}/d_{x^2-y^2}$ vanadium orbitals with a small band curvature plays an important role in the unconventional charge modulation and the superconducting pairing [42]. Among the multiple VHSs, the VHSs from the d_{xz}/d_{yz} orbitals contribute to the nested Fermi surface [37]. The relative positions of VHSs close to E_F would impact the favored charge instability. Then, we illustrate the schematics of the changes in key band structures for $\text{CsV}_{3-x}\text{Mo}_x\text{Sb}_5$, $\text{CsV}_{2.6}\text{Ta}_{0.4}\text{Sb}_5$, and $\text{CsV}_{2.79}\text{Nb}_{0.21}\text{Sb}_5$ compared with CsV_3Sb_5 . In Fig. 5(c), for the Mo-doped case, the VHS₁ remains below the Fermi level and the lifted VHS₂ promotes the nesting condition. In addition, more electrons can tune the Sb band around the Γ point, which pulls down the energy band and gains more density of states for the superconducting pairing. However, the T_c decreases with Mo doping and thus the band near the Γ point has little contribution to the superconductivity in $\text{CsV}_{3-x}\text{Mo}_x\text{Sb}_5$. The suppressed superconductivity may originate from two main effects. One

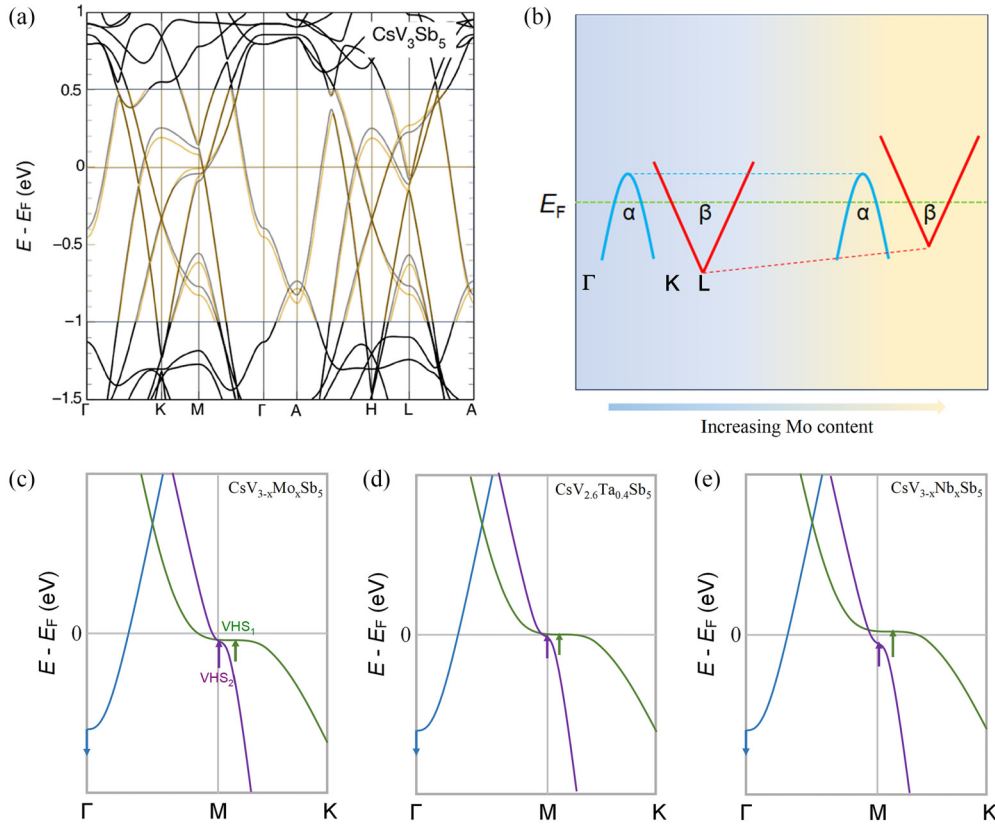


FIG. 5. (a) Calculated band structures of CsV_3Sb_5 and superimposed $\text{CsV}_{2.58}\text{Ta}_{0.42}\text{Sb}_5$ (the yellow lines) above the T_{CDW} , as referred from Ref. [20]. (b) Schematic of the detailed changes in the band structures below the T_{CDW} for $\text{CsV}_{3-x}\text{Mo}_x\text{Sb}_5$. (c)–(e) Schematics of the changes in the key band structures for $\text{CsV}_{3-x}\text{Mo}_x\text{Sb}_5$, $\text{CsV}_{2.58}\text{Ta}_{0.42}\text{Sb}_5$ [18], and $\text{CsV}_{2.79}\text{Nb}_{0.21}\text{Sb}_5$ [17,36], compared with CsV_3Sb_5 , where the arrows represent the shifts of bands compared with CsV_3Sb_5 .

is the impurities that can break the Cooper pair with the introduction of Mo, as reported by the electron-doping cases in $\text{Cs}(\text{V}_{1-x}\text{Cr}_x)_3\text{Sb}_5$ and Cu-doped FeSe [27,43]. The recently nuclear magnetic resonance (NMR) study suggests that the impurity effect has a minor contribution to the suppression of superconductivity [25]. The other is the change of density of states at the Fermi level associated with the enhanced CDW [25]. This suppressed superconductivity could ascribe to the result of a cooperative mechanism.

As shown in Fig. 5(d), for $\text{CsV}_{3-x}\text{Ta}_x\text{Sb}_5$ [18], the enhanced superconductivity is dominated with the shift of VHS_1 by suppressing the competing orders. For $\text{CsV}_{2.79}\text{Nb}_{0.21}\text{Sb}_5$ [17], the high-order VHS_1 crosses the Fermi level after doping and depletes the filled density of states near M leading to the suppression of the CDW, as displayed in Fig. 5(e). Moreover, the downward shift of the band at the Γ point leads to the increase of density of states at the Fermi level [36]. The modifications to the band structures near the Γ and M points make a cooperative promotion of the superconductivity in $\text{CsV}_{3-x}\text{Nb}_x\text{Sb}_5$. On the basis of an opposite shift of the bands near the M and Γ points due to an orbital-selective bandwidth transfer, these results imply that a cooperative mechanism including more introduced electrons and the promoted Fermi-surface nesting would contribute to the unusual competition between the CDW and superconductivity in $\text{CsV}_{3-x}\text{Mo}_x\text{Sb}_5$.

Next, we summarize the unique electronic band structures in $\text{CsV}_{3-x}\text{Mo}_x\text{Sb}_5$. First, the VHSs around the M is slightly

below the Fermi level in pristine CsV_3Sb_5 , by doping Mo into the crystal structure, the VHSs from vanadium orbitals are lifted up and promote the nesting condition. Second, the Fermi surface along the Γ - K direction exhibits a subtle change under Mo doping, which coincides with the ARPES experiments of Ta-doped and Nb-doped systems [18,36]. Third, the Γ -centered Sb electron band is expected to move towards a deeper binding energy under Mo doping performed by more introduced electrons and the change of Hall signal [see Fig. 2(b)].

IV. CONCLUSIONS

In summary, we report comprehensive transport measurements on $\text{CsV}_{3-x}\text{Mo}_x\text{Sb}_5$ single crystals. The intriguing changes in the electronic band structures upon Mo substitution are characterized by the shrinkage of the V-derived band (F_β) forming the van Hove singularity and a subtle change of the band along the Γ - K direction (F_α), and these two Fermi surfaces possess small cyclotron effective masses. The CDW order becomes stronger when the VHSs are close to E_F , revealing that the VHS from d_{xz}/d_{yz} vanadium orbitals plays an important role in the electronic instabilities. In this electron-doped case, the enhanced CDW with Mo substitution is dominated by the promoted Fermi-surface nesting with tunable VHSs at the M point.

ACKNOWLEDGMENTS

We thank Prof. J. He for helpful discussions. This work was supported by the National Nature Science Foundation of China (Grant No. 12074002), the Innovation

Program for Quantum Science and Technology (Grant No. 2021ZD0302802) and Key Project of Natural Scientific Research of Universities in Anhui Province (Grant No. K120462033).

J.S. and T.H. contributed equally to this work.

- [1] Y. Zhou, K. Kanoda, and T. K. Ng, Quantum spin liquid states, *Rev. Mod. Phys.* **89**, 025003 (2017).
- [2] M. L. Kiesel, C. Platt, and R. Thomale, Unconventional Fermi surface instabilities in the kagome Hubbard model, *Phys. Rev. Lett.* **110**, 126405 (2013).
- [3] W. S. Wang, Z. Z. Li, Y. Y. Xiang, and Q. H. Wang, Competing electronic orders on kagome lattices at van Hove filling, *Phys. Rev. B* **87**, 115135 (2013).
- [4] M. L. Kiesel and R. Thomale, Sublattice interference in the kagome Hubbard model, *Phys. Rev. B* **86**, 121105(R) (2012).
- [5] M. Li, Q. Wang, G. Wang, Z. Yuan, W. Song, R. Lou, Z. Liu, Y. Huang, Z. Liu, H. Lei, Z. Yin, and S. Wang, Dirac cone, flat band and saddle point in kagome magnet YMn_6Sn_6 , *Nat. Commun.* **12**, 3129 (2021).
- [6] W. H. Ko, P. A. Lee, and X. G. Wen, Doped kagome system as exotic superconductor, *Phys. Rev. B* **79**, 214502 (2009).
- [7] S.-L. Yu and J.-X. Li, Chiral superconducting phase and chiral spin-density-wave phase in a Hubbard model on the kagome lattice, *Phys. Rev. B* **85**, 144402 (2012).
- [8] B. R. Ortiz, L. C. Gomes, J. R. Morey, M. Winiarski, M. Bordelon, J. S. Mangum, I. W. H. Oswald, J. A. Rodriguez-Rivera, J. R. Neilson, S. D. Wilson, E. Ertekin, T. M. McQueen, and E. S. Toberer, New kagome prototype materials: Discovery of KV_3Sb_5 , RbV_3Sb_5 , and CsV_3Sb_5 , *Phys. Rev. Mater.* **3**, 094407 (2019).
- [9] B. R. Ortiz, S. M. L. Teicher, Y. Hu, J. L. Zuo, P. M. Sarte, E. C. Schueller, A. M. Milinda Abeykoon, M. J. Krogstad, S. Rosenkranz, R. Osborn, R. Seshadri, L. Balents, J. He, and S. D. Wilson, CsV_3Sb_5 : A \mathbb{Z}_2 topological kagome metal with a superconducting ground state, *Phys. Rev. Lett.* **125**, 247002 (2020).
- [10] T. Neupert, M. M. Denner, J. X. Yin, R. Thomale, and M. Z. Hasan, Charge order and superconductivity in kagome materials, *Nat. Phys.* **18**, 137 (2022).
- [11] S. Y. Yang, Y. Wang, B. R. Ortiz, D. Liu, J. Gayles, E. Derunova, R. Gonzalez-Hernandez, L. Šmejkal, Y. Chen, S. S. P. Parkin, S. D. Wilson, E. S. Toberer, T. McQueen, and M. N. Ali, Giant, unconventional anomalous Hall effect in the metallic frustrated magnet candidate, KV_3Sb_5 , *Sci. Adv.* **6**, eabb6003 (2020).
- [12] E. M. Kenney, B. R. Ortiz, C. Wang, S. D. Wilson, and M. J. Graf, Absence of local moments in the kagome metal KV_3Sb_5 as determined by muon spin spectroscopy, *J. Phys.: Condens. Matter* **33**, 235801 (2021).
- [13] M. M. Denner, R. Thomale, and T. Neupert, Analysis of charge order in the kagome metal AV_3Sb_5 ($A = \text{K, Rb, Cs}$), *Phys. Rev. Lett.* **127**, 217601 (2021).
- [14] K. Y. Chen, N. N. Wang, Q. W. Yin, Y. H. Gu, K. Jiang, Z. J. Tu, C. S. Gong, Y. Uwatoko, J. P. Sun, H. C. Lei, J. P. Hu, and J.-G. Cheng, Double superconducting dome and triple enhancement of T_c in the kagome superconductor CsV_3Sb_5 under high pressure, *Phys. Rev. Lett.* **126**, 247001 (2021).
- [15] Y. M. Oey, B. R. Ortiz, F. Kaboudvand, J. Frassinetti, E. Garcia, R. Cong, S. Sanna, V. F. Mitrović, R. Seshadri, and S. D. Wilson, Fermi level tuning and double-dome superconductivity in the kagome metal $\text{CsV}_3\text{Sb}_{5-x}\text{Sn}_x$, *Phys. Rev. Mater.* **6**, L041801 (2022).
- [16] H. Yang, Z. Huang, Y. Zhang, Z. Zhao, J. Shi, H. Luo, L. Zhao, G. Qian, H. Tan, B. Hu *et al.*, Titanium doped kagome superconductor $\text{CsV}_{3-x}\text{Ti}_x\text{Sb}_5$ and two distinct phases, *Sci. Bull.* **67**, 2176 (2022).
- [17] Y. Li, Q. Li, X. Fan, J. Liu, Q. Feng, M. Liu, C. Wang, J. X. Yin, J. Duan, X. Li, Z. Wang, H. H. Wen, and Y. Yao, Tuning the competition between superconductivity and charge order in the kagome superconductor $\text{Cs}(\text{V}_{1-x}\text{Nb}_x)_3\text{Sb}_5$, *Phys. Rev. B* **105**, L180507 (2022).
- [18] Y. Luo, Y. Han, J. Liu, H. Chen, Z. Huang, L. Huai, H. Li, B. Wang, J. Shen, S. Ding *et al.*, A unique van Hove singularity in kagome superconductor $\text{CsV}_{3-x}\text{Ta}_x\text{Sb}_5$ with enhanced superconductivity, *Nat. Commun.* **14**, 3819 (2023).
- [19] T. Qian, M. H. Christensen, C. Hu, A. Saha, B. M. Andersen, R. M. Fernandes, T. Birol, and N. Ni, Revealing the competition between charge density wave and superconductivity in CsV_3Sb_5 through uniaxial strain, *Phys. Rev. B* **104**, 144506 (2021).
- [20] Y. Zhong, J. Liu, X. Wu, Z. Guguchia, J. X. Yin, A. Mine, Y. Li, S. Najafzadeh, D. Das, C. Mielke, III *et al.*, Nodeless electron pairing in CsV_3Sb_5 -derived kagome superconductors, *Nature (London)* **617**, 488 (2023).
- [21] H. Chen, H. Yang, B. Hu, Z. Zhao, J. Yuan, Y. Xing, G. Qian, Z. Huang, G. Li, Y. Ye *et al.*, Roton pair density wave in a strong-coupling kagome superconductor, *Nature (London)* **599**, 222 (2021).
- [22] R. Gupta, D. Das, C. H. Mielke, III, Z. Guguchia, T. Shiroka, C. Baines, M. Bartkowiak, H. Luetkens, R. Khasanov, Q. Yin, Z. Tu, C. Gong, and H. Lei, Microscopic evidence for anisotropic multigap superconductivity in the CsV_3Sb_5 kagome superconductor, *npj Quantum Mater.* **7**, 49 (2022).
- [23] M. Liu, T. Han, X. Hu, Y. Tu, Z. Zhang, M. Long, X. Hou, Q. Mu, and L. Shan, Evolution of superconductivity and charge density wave through Ta and Mo doping in CsV_3Sb_5 , *Phys. Rev. B* **106**, L140501 (2022).
- [24] S. D. Wilson and B. R. Ortiz, AV_3Sb_5 kagome superconductors, *Nat. Rev. Mater.* **9**, 420 (2024).
- [25] K. J. Zhu, L. P. Nie, B. Lei, M. J. Wang, K. L. Sun, Y. Z. Deng, M. L. Tian, T. Wu, and X. H. Chen, Competitive superconductivity and charge density wave in Mo-doped kagome superconductor CsV_3Sb_5 , *Phys. Rev. Res.* **6**, 023295 (2024).
- [26] H. Luo, W. Xie, E. M. Seibel, and R. J. Cava, Superconductivity in $3\text{R-Ta}_{1-x}\text{M}_x\text{Se}_2$ ($M = \text{W, Mo}$), *J. Phys.: Condens. Matter* **27**, 365701 (2015).

- [27] G. Ding, H. Wo, Y. Gu, Y. Gu, and J. Zhao, Effect of chromium doping on superconductivity and charge density wave order in the kagome metal $\text{Cs}(\text{V}_{1-x}\text{Cr}_x)_3\text{Sb}_5$, *Phys. Rev. B* **106**, 235151 (2022).
- [28] Y. Fu, N. Zhao, Z. Chen, Q. Yin, Z. Tu, C. Gong, C. Xi, X. Zhu, Y. Sun, K. Liu, and H. Lei, Quantum transport evidence of topological band structures of kagome superconductor CsV_3Sb_5 , *Phys. Rev. Lett.* **127**, 207002 (2021).
- [29] F. H. Yu, T. Wu, Z. Y. Wang, B. Lei, W. Z. Zhuo, J. J. Ying, and X. H. Chen, Concurrence of anomalous Hall effect and charge density wave in a superconducting topological kagome metal, *Phys. Rev. B* **104**, L041103 (2021).
- [30] B. R. Ortiz, S. M. L. Teicher, L. Kautzsch, P. M. Sarte, N. Ratcliff, J. Harter, J. P. C. Ruff, R. Seshadri, and S. D. Wilson, Fermi surface mapping and the nature of charge-density-wave order in the kagome superconductor CsV_3Sb_5 , *Phys. Rev. X* **11**, 041030 (2021).
- [31] D. Chen, B. He, M. Yao, Y. Pan, H. Lin, W. Schnelle, Y. Sun, J. Gooth, L. Taillefer, and C. Felser, Anomalous thermoelectric effects and quantum oscillations in the kagome metal CsV_3Sb_5 , *Phys. Rev. B* **105**, L201109 (2022).
- [32] C. Broyles, D. Graf, H. Yang, X. Dong, H. Gao, and S. Ran, Effect of the interlayer ordering on the Fermi surface of Kagome superconductor CsV_3Sb_5 revealed by quantum oscillations, *Phys. Rev. Lett.* **129**, 157001 (2022).
- [33] H. Tan, Y. Li, Y. Liu, D. Kaplan, Z. Wang, and B. Yan, Emergent topological quantum orbits in the charge density wave phase of kagome metal CsV_3Sb_5 , *npj Quantum Mater.* **8**, 39 (2023).
- [34] D. Shoenberg, *Magnetic Oscillations in Metals*, Cambridge Monographs on Physics (Cambridge University Press, Cambridge, UK, 1984).
- [35] K. Nakayama, Y. Li, T. Kato, M. Liu, Z. Wang, T. Takahashi, Y. Yao, and T. Sato, Multiple energy scales and anisotropic energy gap in the charge-density-wave phase of the kagome superconductor CsV_3Sb_5 , *Phys. Rev. B* **104**, L161112 (2021).
- [36] T. Kato, Y. Li, K. Nakayama, Z. Wang, S. Souma, F. Matsui, M. Kitamura, K. Horiba, H. Kumigashira, T. Takahashi, Y. Yao, and T. Sato, Fermiology and origin of T_c enhancement in a kagome superconductor $\text{Cs}(\text{V}_{1-x}\text{Nb}_x)_3\text{Sb}_5$, *Phys. Rev. Lett.* **129**, 206402 (2022).
- [37] M. Kang, S. Fang, J. K. Kim, B. R. Ortiz, S. H. Ryu, J. Kim, J. Yoo, G. Sangiovanni, D. D. Sante, B. G. Park, C. Jozwiak, A. Bostwick, E. Rotenberg, E. Kaxiras, S. D. Wilson, J. H. Park, and R. Comin, Twofold van Hove singularity and origin of charge order in topological kagome superconductor CsV_3Sb_5 , *Nat. Phys.* **18**, 301-308 (2022).
- [38] Z. Liu, N. Zhao, Q. Yin, C. Gong, Z. Tu, M. Li, W. Song, Z. Liu, D. Shen, Y. Huang, K. Liu, H. Lei, and S. Wang, Charge-density-wave-induced bands renormalization and energy gaps in a kagome superconductor RbV_3Sb_5 , *Phys. Rev. X* **11**, 041010 (2021).
- [39] Y. Hu, X. Wu, B. R. Ortiz, S. Ju, X. Han, J. Ma, N. C. Plumb, M. Radovic, R. Thomale, S. D. Wilson, A. P. Schnyder, and M. Shi, Rich nature of Van Hove singularities in kagome superconductor CsV_3Sb_5 , *Nat. Commun.* **13**, 2220 (2022).
- [40] Y. Liu, Y. Wang, Y. Cai, Z. Hao, X. M. Ma, L. Wang, C. Liu, J. Chen, L. Zhou, J. Wang, S. Wang, H. He, Y. Liu, S. Cui, B. Huang, J. Wang, C. Chen, and J. W. Mei, Doping evolution of superconductivity, charge order, and band topology in hole-doped topological kagome superconductors $\text{Cs}(\text{V}_{1-x}\text{Ti}_x)_3\text{Sb}_5$, *Phys. Rev. Mater.* **7**, 064801 (2023).
- [41] L. Kautzsch, Y. M. Oey, H. Li, Z. Ren, B. R. Ortiz, G. Pokharel, R. Seshadri, J. Ruff, T. Kongruengkit, J. W. Harter, Z. Wang, I. Zeljkovic, and S. D. Wilson, Incommensurate charge-stripe correlations in the kagome superconductor $\text{CsV}_3\text{Sb}_{5-x}\text{Sn}_x$, *npj Quantum Mater.* **8**, 37 (2023).
- [42] C. Lin, A. Consiglio, O. K. Forslund, J. Kuspert, M. M. Denner, H. Lei, A. Louat, M. D. Watson, T. K. Kim, C. Cacho *et al.*, Giant strain response of charge modulation and singularity in a kagome superconductor, [arXiv:2402.16089](https://arxiv.org/abs/2402.16089).
- [43] C. Gong, S. Sun, S. Wang, and H. Lei, Normal and superconducting state properties of Cu-doped FeSe single crystals, *Phys. Rev. B* **103**, 174510 (2021).